Bioorganic & Medicinal Chemistry xxx (2016) xxx–xxx

Contents lists available at ScienceDirect

Bioorganic & Medicinal Chemistry

journal homepage: www.elsevier.com/locate/bmc

Discovery, design and synthesis of 6*H*-anthra[1,9-*cd*]isoxazol-6-one scaffold as G9a inhibitor through a combination of shape-based virtual screening and structure-based molecular modification

Wei-Lin Chen [a], Zhi-Hui Wang [a], Tao-Tao Feng [a], Dong-Dong Li [a], Chu-Hui Wang [a], Xiao-Li Xu [a,b], Xiao-Jin Zhang [a,b,c], Qi-Dong You [a,b,*], Xiao-Ke Guo [a,b,*]

[a] *State Key Laboratory of Natural Medicines and Jiangsu Key Laboratory of Drug Design and Optimization, China Pharmaceutical University, Nanjing 210009, China*
[b] *Department of Medicinal Chemistry, School of Pharmacy, China Pharmaceutical University, Nanjing 210009, China*
[c] *Department of Organic Chemistry, School of Science, China Pharmaceutical University, Nanjing 210009, China*

ARTICLE INFO

Article history:
Received 31 August 2016
Revised 29 September 2016
Accepted 29 September 2016
Available online xxxx

Keywords:
Histone methyltransferases
G9a inhibitor
Virtual screening
Structure–activity relationship
Anti-cancer

ABSTRACT

Protein lysine methyltransferase G9a is widely considered as an appealing antineoplastic target. Herein we present an integrated workflow combining shape-based virtual screening and structure-based molecular modification for the identification of novel G9a inhibitors. The shape-based similarity screening through ROCS overlay on the basis of the structure of **UNC0638** was performed to identify **CPUY074001** contained a 6*H*-anthra[1,9-*cd*]isoxazol-6-one scaffold as a hit. Analysis of the binding mode of **CPUY074001** with G9a and 3D-QSAR results, two series compounds were designed and synthesized. The derivatives were confirmed to be active by in vitro assay and the SAR was explored by docking stimulations. Besides, several analogues showed acceptable anti-proliferative effects against several cancer cell lines. Among them, **CPUY074020** displayed potent dual G9a inhibitory activity and anti-proliferative activity. Furthermore, **CPUY074020** induced cell apoptosis in a dose-dependent manner and displayed a significant decrease in dimethylation of H3K9. Simultaneously, **CPUY074020** showed reasonable in vivo PK properties. Altogether, our workflow supplied a high efficient strategy in the identification of novel G9a inhibitors. Compounds reported here can serve as promising leads for further study.

© 2016 Published by Elsevier Ltd.

1. Introduction

Reversible methylation of histone lysine residues, which is regulated by histone methyltransferases (HMTs) and histone demethylases (HDMs), plays an important role in epigenetic gene expression.[1] G9a (also known as KMT1C (lysine methyltransferase 1C) or EHMT2 (euchromatic histone methyltransferase 2)) was initially identified as a lysine methyltransferase (KMT) which was responsible for catalyzing the mono-, di- and slowly trimethylation of histone H3 lysine 9 (H3K9).[2–7] Increasing evidence suggested that G9a played crucial roles in many biological progresses including gene expression, transcriptional regulation, cell differentiation, proliferation, senescence and replication.[2–8] The fact that G9a mediates complex biological functions and is overexpressed in human cancers including leukemia,[9] prostate carcinoma,[10,11] hepatocellular carcinoma[12] and lung cancer.[13] It has been shown that knockdown of G9a inhibited cancer cell growth.[11,14] It was later found that G9a could methylate various histone[15] and non-histone proteins including the tumor suppressor p53, which was implicated in over 50% of cancers.[10] These observations suggest that inhibition of G9a could be a validated therapeutic strategy against cancers.

Till now, there are only three chemical types small molecular inhibitors had been reported (Fig. 1), and these inhibitors of G9a were mainly focused on quinazoline scaffold (**UNC0638**).[16] Besides, the discovery approaches can be just summarized as high throughput screening (HTS) and optimization of known inhibitors such as **BIX-01294**.[17,18] Up to now, no inhibitor is advanced to clinical trials, which may result of the poor in vivo pharmacokinetic properties of reported compounds. Therefore, it is urgent to discovery novel chemical scaffolds for the study of therapeutic and biological roles of G9a in various diseases.

Ligand-based virtual screening of large compound databases has been proved to be an effective method in discovery novel hits for a certain target.[19–21] For instance, the OMEGA/ROCS (OpenEye Scientific Software, Inc.) method represented an efficient

* Corresponding authors. Tel./fax: +86 025 83271351.
E-mail addresses: youqidong@gmail.com (Q.-D. You), kexin95@126.com (X.-K. Guo).

http://dx.doi.org/10.1016/j.bmc.2016.09.071
0968-0896/© 2016 Published by Elsevier Ltd.

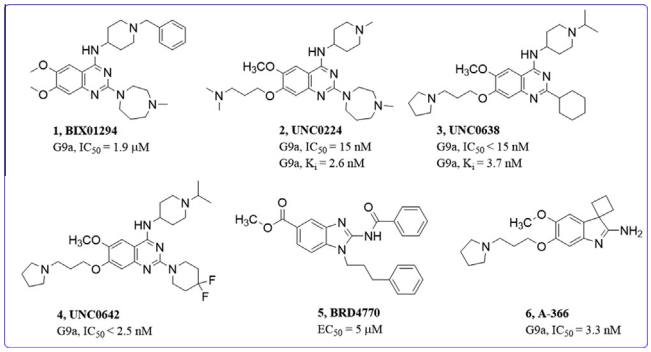

Figure 1. Representative structures of known inhibitors of G9a.

strategy.[22,23] To the best of our knowledge, no study has been published about identification of G9a inhibitory compounds using virtual screening (VS) method. Besides, several crystals of G9a have been solved making a VS approach possible. With the aim of acquiring novel scaffolds of G9a inhibitors, this present work, we firstly developed a virtual screening model on the basis of **UNC0638** by using the ROCS.[22,23] The model was then applied to screen the ChemDiv database, resulting in compound **CPUY074001** with moderate inhibitory activity against G9a. Guided by the binding mode of **CPUY074001** to G9a and 3D-QSAR results[24], we designed, synthesized two series of derivatives and evaluated G9a inhibitory activity using Alphascreen assay. The representative compounds were evaluated antitumor activities in multiple cancer cell lines. Subsequently, compound **CPUY074020**, with promising G9a inhibitory activity and anti-proliferative activity, was verified to induce cell death through apoptosis. The cellular activity was confirmed by analyzing the H3K9me2 and H3K9me3 methylation in western blotting. What's more, the pharmacokinetic parameters of **CPUY074020** in mice were reasonable. Thus, compound **CPUY074020** containing a 6*H*-anthra[1,9-*cd*]isoxazol-6-one scaffold may represent a novel structure displaying inhibition activity against G9a. The discovery workflow of the new scaffold was shown in Figure 2.

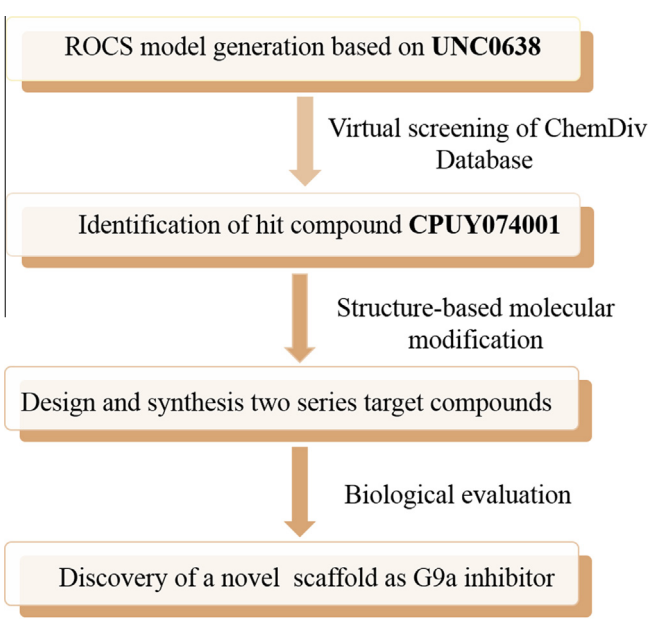

Figure 2. Overview of the molecular modeling workflow.

2. Results and discussion

2.1. ROCS model generation based on UNC0638 and virtual screening

ROCS represents heavy atoms by Gaussians with parametrized decay constants according to the respective van der Waals radii. This representation of atoms allows a fast shape comparison of molecules due to the straightforward calculation of molecular overlaps providing sufficient speed for virtual screening of large database.[25] Some studies also suggested that selecting of an appropriate query for shape-based screening was very important as it affected the virtual screening performance.[26,27] In most cases, the query for the shape similarity search was generated from highly potent small molecule inhibitors of the protein. These findings encouraged us to employ this complementary methodology as a screening model for identification of novel scaffolds that possessed similar structures with **UNC0638**. **UNC0638** was selected as a reference molecule in a shape similarity analysis to identify compounds for three reasons: (1) **UNC0638** was a potent inhibitor for G9a and showed high activity in cells. (2) It also exhibited selectivity against G9a and GLP over a wide range of epigenetic and non-epigenetic targets. (3) A high resolution co-crystal structure of the G9a–**UNC0638** complex has been obtained. The bioactive conformation of **UNC0638** can promote to develop shape based screening. The structure of **UNC0638** was separated from the co-crystal complex (PDB code: 3RJW) and directly used to generate the ROCS query. The key scaffold of **UNC0638** was defined by its quinazoline core. The tertiary amine group was described as cations. The polar atom such as the nitrogen of pyrimidine, 6-oxygen atom and 7-oxygen atom were defined as hydrogen bond acceptors. 4-Secondory amine group was defined as hydrogen donor, respectively. The molecular shape of **UNC0638** was depicted in a cyan shadow (Fig. 3). Further exploration of database using the model would lead to compounds with similar chemical property and molecular shape to **UNC0638**.

2.2. Identification of the hit compound CPUY074001

To identify novel G9a inhibitors scaffold targeting the catalytic site, a virtual screening procedure was employed and followed by biological testing of the identified compounds. For the ChemDiv database, the multiple conformations of different query molecules were calculated using OMEGA with a maximum of 400 conformations.[28,29] Initially, each molecule in these conformational database was aligned with the query and scored for 3D shape overlap using ROCS. Then, the 3D shape-based similarity of a given compound to **UNC0638** was ranked by a combined scoring method. The selection was based on two criteria: (i) compounds were available at the time of our study and (ii) showed sufficient structural diversity among each other. Much to our delight, **CPUY074001**, with a 6*H*-anthra[1,9-*cd*]isoxazol-6-one scaffold, showed 39.34% inhibition against G9a under 10 μM and with IC_{50} value of 39.19 ± 0.73 μM.

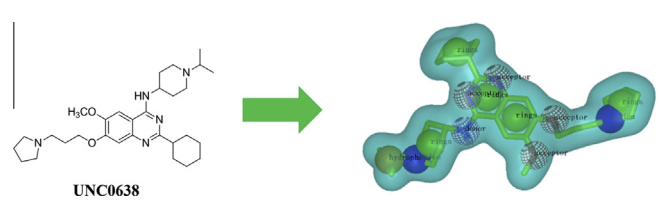

Figure 3. ROCS shape query derived from **UNC0638**. The green spheres illustrate ROCS ring features, the red spheres illustrate hydrogen bond acceptors, the gray sphere illustrates hydrogen bond donors, and the blue spheres illustrate cations.

The binding pattern of **CPUY074001** with G9a was analyzed by molecular docking using CDOKER module inbuilt in DS 3.0. The bulk of **CPUY074001** occupied the histone peptide binding site. Two hydrogen bonds were observed: one was between the 6-carbonyl and Asp1088, a residue in the region of active site; another was from the nitrogen atom and oxygen atom of isoxazole ring to Asp 1078. The tetracyclic scaffold was surrounded by the hydrophobic residues such as Ile1072, Ala1077, Leu108, Val1096 and Cys1098. The tetracyclic scaffold interacted with these residues by forming van der Waals force (Fig. 4A). The binding pattern was also depicted by the 'surface around ligand' mode. It can be easily observed that **CPUY074001** can occupy the active cavity well in a reasonable conformation and the tetracyclic scaffold occupied the hydrophobic pocket. In addition to this, the 5-*p*-methoxyphenyl side chain of it interacted with the lysine binding channel of G9a (Fig. 4B). The binding mode analysis clearly explained the activity of **CPUY074001** and indicated it can serve as a proper hit for further optimization.

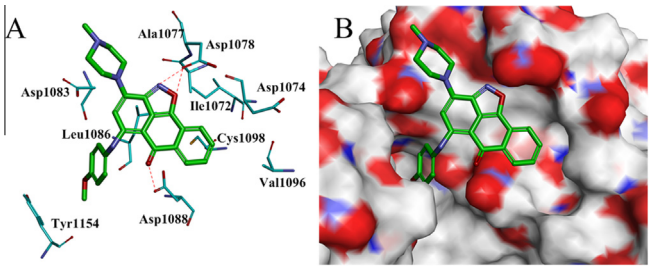

Figure 4. The binding pattern analysis of **CPUY074001** to G9a. The key residues (A) and the protein surface (B) around **CPUY074001** were shown, respectively. Compound **CPUY074001** was shown as cylinders with carbon atoms in green. The H-bonds were shown as red dot lines. The surface was colored by the electrostatic state of the residues.

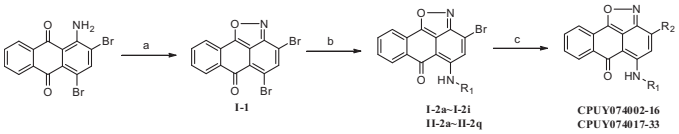

Scheme 1. Synthesis route of **CPUY074002-16**. Reagents and conditions (a) $NaNO_2$/H_2SO_4, NaN_3, toluene, reflux, 16 h; (b) R_1NH_2, $AlCl_3$, DCM, 40 °C, 12 h; (c) R_2, acetonitrile, 80 °C, 2 h.

2.3. Optimization of the hit compound CPUY074001

In order to investigate the effect of G9a inhibitory activities of different substitutions on the phenyl ring and R_2 groups, we designed and synthesized series I compounds (**CPUY074002**–**CPUY074016**). The synthesis route of this series of compounds were outlined in Scheme 1. The 3,5-dibromo-6*H*-anthra[1,9-*cd*]isoxazol-6-one (**I-1**) was obtained by the diazotization reaction. The intermediate **I-1** were substituted at the 5-position with various aromatic amine to give arylamination of **I-2a**–**I-2i**. Then a second amination was carried out at the 3-position using refluxing acetonitrile to provide a moderate yield of target compounds **CPUY074002**–**16**.[30]

The synthesized compounds **CPUY074002**–**16** were initially evaluated for inhibition of G9a activity at 10 μM using AlphaScreen assay, while **UNC0638** was used as a positive control for the experiment. As shown in Table 1, most of the compounds possessed similar bioactivity to the hit **CPUY074001**. Replacement of 4-methoxylphenyl (**CPUY074001**, **CPUY074002** and **CPUY074003**) with 4-methylphenyl (**CPUY074006**, **CPUY074007** and **CPUY074008**) displayed equal inhibition activity against G9a. The existence of electron withdrawing group (–CN, –F) at the 4-position in phenyl moiety demonstrated superior inhibition against G9a (**CPUY074002** vs **CPUY074009**), (**CPUY074003** vs **CPUY074012**). While $-OCF_3$ group at 4-position in phenyl moiety diminished the activity (**CPUY074005** vs **CPUY074016**). On the whole, the modification of series I was less than satisfactory. None of the compounds was superior to hit compound **CPUY07001** a lot. All of them displayed the moderate G9a inhibition. This result indicated that introducing a bulk group at the 5-position was not tolerate. Thus, we proceeded to further optimize.

Table 1
G9a inhibition profile of series I compounds

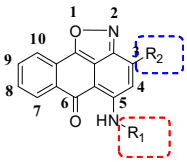

Compd	R_1	R_2	G9a % inhibition @ 10 μM[a]
CPUY074001	4-Methoxylphenyl	4-Methylpiperazinyl	39.34
CPUY074002	4-Methoxylphenyl	Dimethylamino	19.11
CPUY074003	4-Methoxylphenyl	4-Ethylpiperazinyl	40.18
CPUY074004	4-Methoxylphenyl	Pyrrolidinyl	40.91
CPUY074005	4-Methoxylphenyl	4-Phenylpiperazinyl	26.07
CPUY074006	4-Methylphenyl	Dimethylamino	15.13
CPUY074007	4-Methylphenyl	4-Methylpiperazinyl	31.67
CPUY074008	4-Methylphenyl	4-Ethylpiperazinyl	40.21
CPUY074009	4-Cyanlphenyl	Dimethylamino	34.26
CPUY074010	4-Chlorophenyl	4-Methylpiperazinyl	26.86
CPUY074011	2-Fluorophenyl	Dimethylamino	22.36
CPUY074012	2-Fluorophenyl	4-Ethylpiperazinyl	48.72
CPUY074013	3-Fluorophenyl	4-Methylpiperazinyl	21.95
CPUY074014	4-Fluorophenyl	4-Methylpiperazinyl	37.67
CPUY074015	2,4-Difluorophenyl	4-Methylpiperazinyl	9.77
CPUY074016	4-Trifluoromethoxyphenyl	4-Phenylpiperazinyl	16.12
UNC0638	–	–	98.02

[a] Values are means of at least two experiments.

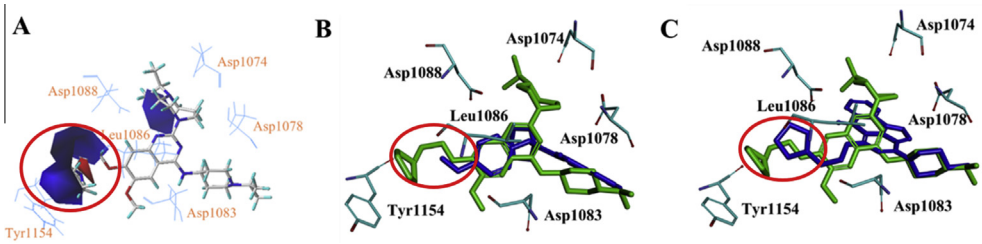

Figure 5. (A) The binding pattern of compound **33** with CoMSIA electrostatic field: contour maps of CoMSIA electrostatic field superimposed into the active binding site of G9a and compound **33** was in the binding site of G9a. (B) The superimposition of compound **33** with **CPUY074001**. Compound **33** was shown as cylinders in green and **CPUY074001** in blue. (C) The superimposition of compound **33** with **CPUY07017**. Compound **33** was shown as cylinders in green and **CPUY074017** in blue.

No significant inhibitory activity variation was observed when changing the substitution in the phenyl ring, demonstrating a structural tolerance at this position. Inspired by the docking result of **CPUY074001** (Fig. 4) and 3D-QSAR result (Fig. 5A),[24] we speculated this site was favorable for positively charged groups. Hence, we kept the tetracyclic scaffold and firstly turned our attention to the modification of the 5-position at the scaffold.

The series II compounds (**CPUY074017–CPUY074033**) were prepared using the similar synthetic procedure of series I compounds, with replacement of the aniline by corresponding aliphatic amine **II-2a–II-2q** (Scheme 1). The inhibitory activity against G9a at 10 μM were also evaluated using Alphascreen assay. The IC_{50} values were further determined from concentration–response curve established by cumulatively applying ten escalating concentrations (0.1 nM–10 μM) of the test compounds. The IC_{50} was determined from two independent experiments and reported as mean ± SD. Interestingly, compounds of series II showed much improved activities compared to compounds of series I (Table 2). Replacing 4-methoxylphenyl at the 5-position with pyrrolidinylethyl group significantly improved the activity (IC_{50} = 39.19 ± 0.73 μM, **CPUY074001** vs IC_{50} = 6.89 ± 1.45 μM, **CPUY074017**). Compared with the hit compound, **CPUY074017** exhibited a better superimposition to the quinazoline inhibitor **33** (Fig. 5B and C).[24] This result validated our previous hypothesis and enabled structure-based optimization of this novel scaffold G9a inhibitors. In order to deeply understand the binding mode of our compounds with G9a, the docking simulations were performed to analyze the most active compounds **CPUY074019**, **CPUY074020** and **CPUY074030** bound to G9a. As illustrated in Figure 6, both of **CPUY074019** and **CPUY074020** showed the same

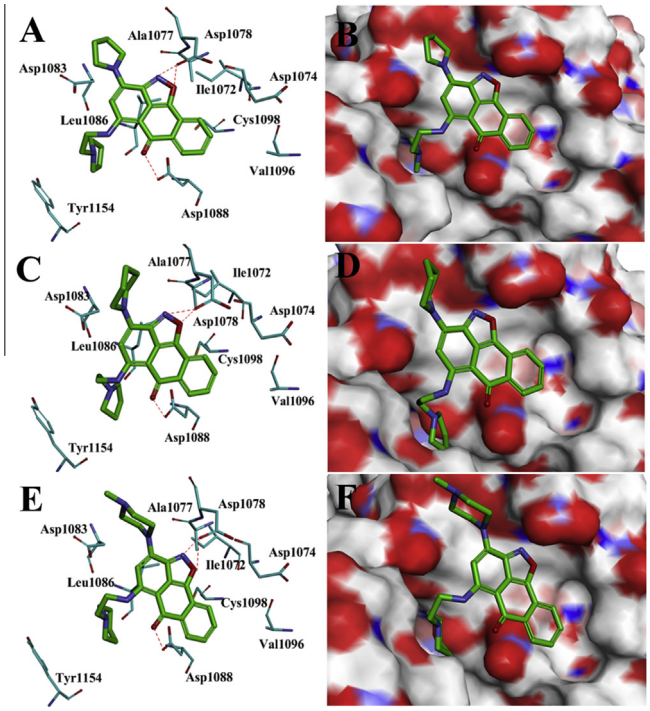

Figure 6. The binding pattern analysis of **CPUY074019** (A and B), **CPUY074020** (C and D), **CPUY074030** (E and F) to G9a. The key residues (A, C and E) and the protein surface (B, D and F) were shown respectively. Compounds were shown as cylinders with carbon atoms in green. The H-bonds were shown as red dot lines. The surface was colored by the electrostatic state of the residues.

Table 2
G9a inhibition profile of series II compounds

Compd	R_1	R_2	G9a % inhibition @ 10 μM[a]	G9a (IC_{50}, μM)
CPUY074017	Pyrrolidinylethyl	4-Methylpiperazinyl	62.93	6.89 ± 1.45
CPUY074018	Pyrrolidinylethyl	Dimethylamino	69.21	3.87 ± 1.92
CPUY074019	Pyrrolidinylethyl	Pyrrolidinyl	92.02	1.22 ± 0.13
CPUY074020	Pyrrolidinylethyl	Piperidino	91.52	2.18 ± 0.013
CPUY074021	Pyrrolidinylethyl	4-Ethylpiperazinyl	70.58	3.48 ± 0.36
CPUY074022	Pyrrolidinylethyl	4-(2-Pyrimidyl)piperazinyl	70.01	4.57 ± 0.64
CPUY074023	Pyrrolidinylethyl	4-Phenylpiperazinyl	87.14	3.22 ± 0.14
CPUY074024	Pyrrolidinylethyl	4-Methylhomopiperazinyl	63.92	3.96 ± 0.54
CPUY074025	*N,N*-Dimethylaminoethyl	Dimethylamino	64.31	3.47 ± 0.31
CPUY074026	*N,N*-Dimethylaminoethyl	Piperidino	81.51	3.75 ± 0.24
CPUY074027	*N,N*-Dimethylaminoethyl	Pyrrolidinyl	60.98	5.97 ± 0.32
CPUY074028	*N,N*-Dimethylaminoethyl	4-Methylpiperazinyl	63.69	4.84 ± 0.38
CPUY074029	*N,N*-Dimethylaminoethyl	4-(2-Pyrimidyl)piperazinyl	60.99	3.84 ± 0.035
CPUY074030	Piperidinoethyl	4-Methylpiperazinyl	79.01	1.87 ± 0.19
CPUY074031	Piperidinoethyl	4-Methylhomopiperazinyl	64.28	2.49 ± 0.13
CPUY074032	Piperidinoethyl	4-Phenylpiperazinyl	72.21	2.68 ± 0.089
CPUY074033	1-Pyrrolidinylpropyl	Dimethylamino	71.54	2.98 ± 0.22
UNC0638	—	—	98.02	0.61 ± 0.17

[a] Values are means of at least two experiments.

binding pattern to G9a with **CPUY074001**, except for the difference that the N-atom at the pyrrolidinylethyl of them formed electrostatic force with carboxyl groups of Asp1083 and Asp1088 (Fig. 6A and C). This difference also appeared in piperidinoethyl of **CPUY074030** (Fig. 6E). These observations may explain the higher G9a inhibition of series II compounds, revealing the flexible side chains containing terminal tertiary amine in R_1 were essential for G9a inhibition activity. Molecular surface visualization showed that all of them occupied the cavities well in a reasonable conformation (Fig. 6B, D and F).

We kept R_2 group and changed R_1 group from *N*,*N*-dimethylaminoethyl to pyrrolidinylethyl leading to **CPUY074018** with no significant variation (IC_{50} = 3.47 μM, **CPUY074025** vs IC_{50} = 3.87 μM, **CPUY074018**). In keeping with this, the pyrrolidinylethyl substituent at R_1 (**CPUY074023**, IC_{50} = 3.22 μM) showed similar inhibition with piperidinoethyl substituent compound (**CPUY074032**, IC_{50} = 2.68 μM). The binding mode also demonstrated different steric modifications had no effect on electrostatic force between carboxyl groups of Asp1083, Asp1088 and N-atom at R_1 substitution (**CPUY074019** vs **CPUY074030**), suggesting that the R_1 position could bear different steric modifications.

With the aim to further investigate the effect of 3-position substituents, we replaced 4-methylpiperazinyl group (**CPUY074017**, IC_{50} = 6.89 μM) with dimethylamino (**CPUY074018**, IC_{50} = 3.87 μM), piperidino (**CPUY074019**, IC_{50} = 1.22 μM) and pyrrolidinyl (**CPUY074020**, IC_{50} = 2.18 μM) enhancing the inhibition against G9a slightly. Meanwhile, the similar observation could also be detected between **CPUY074028** (IC_{50} = 4.84 μM) and **CPUY074025** (IC_{50} = 3.47 μM), **CPUY074026** (IC_{50} = 3.75 μM), demonstrating the terminal tertiary amine substituents at 3- position were not required for the activity. Compared to **CPUY074030** (IC_{50} = 1.87 μM) compounds with bulky groups at 3-position, such as 4-methylhomopiperazinyl (**CPUY074031**, IC_{50} = 2.49 μM) and 4-phenylpiperazinyl (**CPUY074032**, IC_{50} = 2.68 μM), led to slightly loss of activity, indicating that it was not suitable to introduce large groups of R_2 substituents. In this series, all of the compounds significantly improved G9a inhibitory activity compared to the hit compound and showed equal activity to the positive control **UNC0638**.

2.4. Anti-proliferative activities evaluation of representative compounds

Anti-proliferative activities of representative potent compounds were performed with cell survival being determined by the 3-(4,5-dimethylthiazol-2-yl)-2,5-diphenyltetrazolium bromide (MTT) colorimetric assay against HCT116 (colon cancer), MCF-7 (breast cancer) and HepG2 (liver cancer) cells. **UNC0638** was used as a positive control. As shown in Table 3, it was found that all the compounds of series II showed moderate or potent anti-proliferative activity against three cancer cell lines, while the compounds of series I showed barely anti-proliferative activity. This might be ascribed to their inferior aqueous solubility. The anti-proliferation activities of these compounds were consistent with their target-based data. To our delight, some compounds (**CPUY074022**, **CPUY074023**, **CPUY074029**, **CPUY074031** and **CPUY074032**) showed comparable activities against MCF-7 cell line to the positive control with IC_{50} values ranging from 1.22 to 5.08 μM. It was worth noting that **CPUY074020** exhibited slightly improved activity against both HCT116 and MCF-7 cell lines than **UNC0638**. Taking all data into account, compound **CPUY074020** was selected for further evaluation of the cellular activities.

Table 3
Cell anti-proliferative activity of the indicated compounds

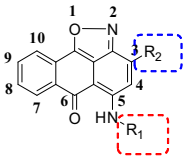

Compd	R_1	R_2	Cell viability IC_{50} (μM)		
			HCT116	MCF-7	HepG2
CPUY074001	4-Methoxylphenyl	4-Methylpiperazinyl	139.50 ± 24.12	>200	>200
CPUY074003	4-Methoxylphenyl	4-Ethylpiperazinyl	>200	>200	>200
CPUY074004	4-Methoxylphenyl	Pyrrolidinyl	>200	>200	66.66 ± 5.08
CPUY074008	4-Methylphenyl	4-Ethylpiperazinyl	>200	>200	>200
CPUY074012	2-Fluorophenyl	4-Ethylpiperazinyl	>200	>200	>200
CPUY074017	Pyrrolidinylethyl	4-Methylpiperazinyl	6.23 ± 1.15	13.92 ± 1.11	27.79 ± 1.08
CPUY074018	Pyrrolidinylethyl	Dimethylamino	6.99 ± 1.05	27.99 ± 7.11	24.85 ± 2.41
CPUY074019	Pyrrolidinylethyl	Pyrrolidinyl	7.46 ± 0.21	10.78 ± 1.15	24.95 ± 2.03
CPUY074020	Pyrrolidinylethyl	Piperidino	3.18 ± 1.33	4.52 ± 0.93	7.93 ± 1.40
CPUY074021	Pyrrolidinylethyl	4-Ethylpiperazinyl	4.34 ± 1.12	20.78 ± 3.61	8.32 ± 0.98
CPUY074022	Pyrrolidinylethyl	4-(2-Pyrimidyl)piperazinyl	3.36 ± 0.41	4.06 ± 0.61	3.10 ± 0.14
CPUY074023	Pyrrolidinylethyl	4-Phenylpiperazinyl	4.28 ± 0.72	3.77 ± 0.42	10.75 ± 2.25
CPUY074024	Pyrrolidinylethyl	4-Methylhomopiperazinyl	3.20 ± 0.14	8.26 ± 1.05	9.35 ± 1.16
CPUY074025	*N*,*N*-Dimethylaminoethyl	Dimethylamino	30.68 ± 2.64	16.58 ± 6.71	12.26 ± 1.73
CPUY074026	*N*,*N*-Dimethylaminoethyl	Piperidino	25.43 ± 1.38	10.29 ± 1.23	15.55 ± 0.91
CPUY074027	*N*,*N*-Dimethylaminoethyl	Pyrrolidinyl	52.85 ± 17.18	17.64 ± 4.93	20.49 ± 4.97
CPUY074028	*N*,*N*-Dimethylaminoethyl	4-Methylpiperazinyl	18.24 ± 1.87	10.83 ± 0.41	28.58 ± 2.62
CPUY074029	*N*,*N*-Dimethylaminoethyl	4-(2-Pyrimidyl)piperazinyl	4.39 ± 1.02	4.31 ± 0.30	9.14 ± 0.36
CPUY074030	Piperidinoethyl	4-Methylpiperazinyl	4.56 ± 0.39	8.37 ± 0.36	8.34 ± 1.04
CPUY074031	Piperidinoethyl	4-Methylhomopiperazinyl	3.96 ± 0.38	5.08 ± 0.91	6.21 ± 0.16
CPUY074032	Piperidinoethyl	4-Phenylpiperazinyl	5.32 ± 1.10	1.22 ± 0.15	10.36 ± 3.01
CPUY074033	1-Pyrrolidinylpropyl	Dimethylamino	11.34 ± 1.47	8.61 ± 0.31	16.94 ± 1.76
UNC0638	—	—	3.35 ± 1.21	6.99 ± 0.79	3.70 ± 2.06

2.5. Effects of CPUY074020 on cell apoptosis

In order to identify whether **CPUY074020** induced cell death through apoptosis, a morphological observation study was used to evaluate its influence on cell skeleton and Hoechst 33258 staining was taken to evaluate nuclei condensation. Under the inverted light microscope (×200), incubation of 2 μM, 4 μM and 8 μM of **CPUY074020** for 24 h resulted in phenotypic changes of MCF-7 cells, such as distortion, membrane blebbing and shrinkage under 4 μM, and vast majority of cells became round in shape and necrosis at 8 μM, while cells in untreated group grew well (Fig. 7A). Meanwhile, Hoechst staining demonstrated the dose-dependent apoptotic bodies appeared (arrow pointing) after treatment with **CPUY074020**, (Fig. 7B) which is commonly accepted as a marker of apoptosis. The annexin V staining assay also proved this result (Fig. 7C). **CPUY074020** induced MCF-7 cells apoptosis, confirming our compounds may be promising novel anti-cancer agents.

2.6. Western-blot analysis of CPUY074020

To further characterize 6*H*-anthra[1,9-*cd*]isoxazol-6-one scaffold compounds as potential G9a inhibitors and evaluate the cellular activity, MCF-7 cells were treated with 2.5 μM, 5 μM and 10 μM of compound **CPUY074020** for 48 h and 2.5 μM of **UNC0638** was selected as positive control. Equivalent amounts of protein from cell extracts were Western Blotted for H3K9me2 and H3K9me3, using β-actin as a loading control, and DMSO as a negative control. A significant decrease in dimethylation level of H3K9 was observed after treatment with 2.5 μM of **CPUY074020**. The result showed that **CPUY074020** dose-dependently de-regulated H3K9 trimethylation (Fig. 8). This data further verified the enzyme-based and cell-based evaluation results and paved the way for in vivo study.

2.7. Assessment of in vivo PK properties of CPUY074020

In order to investigate the PK properties of these novel compounds, **CPUY074020**, with good potencies in vitro, was selected for evaluation of its in vivo PK properties in mice. The compound exhibited reasonable PK properties, with an oral bioavailability of 55.5% and a $T_{1/2}$ value of 4.0 h at an oral dose of 10 mg/kg (Table 4). The compound exposure was also reasonable with an AUC = 723.8 μg/L·h. It had a similar PK properties at the i.v. dosing protocol (Table 4). Taken together, these encouraging PK results suggested that **CPUY074020** may serve as a promising starting point for further optimization leading to in vivo study.

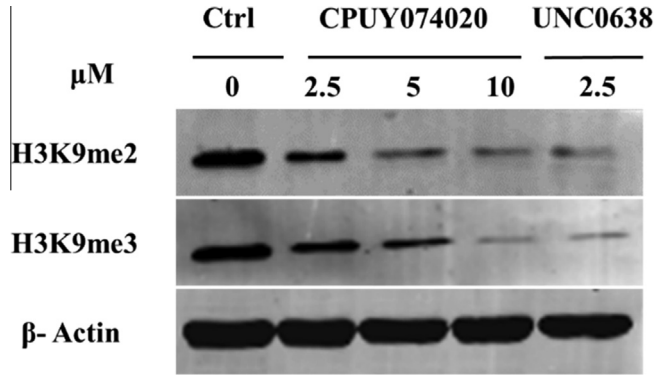

Figure 8. Western blot analysis of H3K9me2 and H3K9me3 methylation after treatment of MCF-7 cells with compound **CPUY074020**.

Table 4
In vivo PK properties of **CPUY074020**

PK parameters	po	iv
AUC[a] (μg/L·h)	723.8 ± 248.8	1304.9 ± 317.6
$t_{1/2}$[a] (h)	4.0 ± 0.9	6.9 ± 0.8
T_{max}[a] (h)	6.7 ± 2.1	0.12 ± 0.19
C_{max}[a] (μg/L)	70.7 ± 29.6	188.2 ± 35.0
Cl[a] (L/h/kg)	15.2 ± 5.2	8.1 ± 2.1
V[a] (L/kg)	90.7 ± 39.5	80.2 ± 20.2
F %	55.5	

[a] Data are expressed as mean ± SD, *n* = 6.

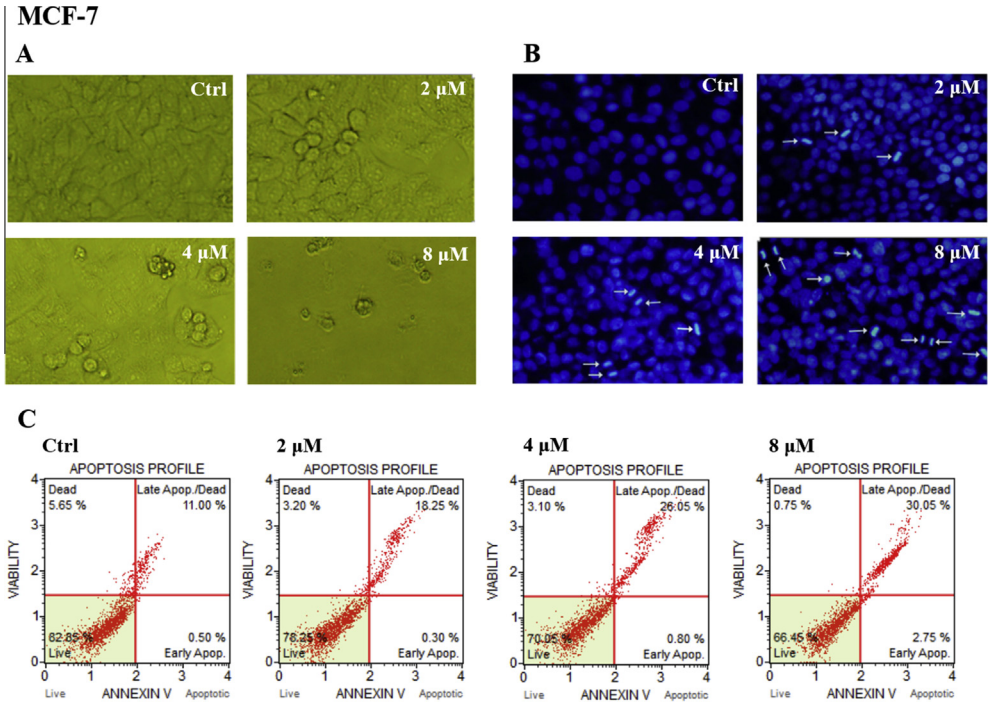

Figure 7. Morphologic changes of the whole cancer cells (A) and the nuclei (B) after treatment of MCF-7 with **CPUY074020**. The arrow pointed to apoptotic bodies. (C) Cell apoptosis were analyzed by annexin V/staining.

3. Conclusions

Using the shape-based virtual screening and structure-based modifications, here we reported two series of compounds with novel scaffold as potential G9a inhibitors. The shape-based screening model was built using the ROCS method, based on the structure of **UNC0638**. By using the model, we identified a hit compound **CPUY074001** with 6*H*-anthra[1,9-*cd*]isoxazol-6-one chemical scaffold exhibited promising inhibitory activities against G9a. Subsequently, we designed, synthesized and evaluated two series of derivatives by modifying the hit compound. Different substituents were introduced at 3- and 5-position via analysis of the docking results and 3D-QSAR results. All compounds of series II, which replaced the aniline groups at 5-position by aliphatic amine with flexible side chains, performed significantly improved G9a inhibitory activity. Furthermore, our docking simulation indicated that their improved activities may mainly result from the electrostatic force between N-atom at the terminal tertiary amine of R_1 substituents and carboxyl groups of Asp1083 and Asp1088. Additionally, we also evaluated anti-proliferative activities of selected compounds on three tumor cell lines of HCT116, MCF-7 and HepG2. To our delight, their anti-proliferative activities were consistent with enzyme-based activities and series II compounds showed promising anti-proliferative activities. **CPUY074020** was selected for further cellular assay and PK test for its excellent G9a inhibitory activity and anti-proliferative activity. The results showed that **CPUY074020** may induce cell death through apoptosis. The decrease levels of H3K9me2 and H3K9me3 in MCF-7 cells suggested **CPUY074020** inhibition of G9a was on-target. Simultaneously, **CPUY074020** displayed reasonable PK properties in mice. In conclusion, here we provided a novel chemical scaffold targeted for G9a, which can be further optimized as G9a chemical tool and therapeutic agents. Besides, the virtual screen method can also be used to screen existing database to identify derivatives with desired activity, which may be a new efficient strategy for identification of novel potential G9a inhibitors.

Acknowledgments

This work was supported by the Project Program of State Key Laboratory of Natural Medicines, China Pharmaceutical University (SKLNMZZCX201611), National Natural Science Foundation of China (81230078, 81573346), National Major Science and Technology Project of China (Innovation and Development of New Drugs) (2013ZX09402102-001-005, 2014ZX09507002-005-015), Specialized Research Fund for the Doctoral Program of Higher Education (20130096110002), Priority Academic Program Development of Jiangsu Higher Education Institutions and National Natural Science Foundation of China (81502915, youth foundation).

Supplementary data

Supplementary data associated with this article can be found, in the online version, at http://dx.doi.org/10.1016/j.bmc.2016.09.071.

References and notes

1. Bannister, A. J.; Kouzarides, T. *Nature* **2005**, *436*, 1103.
2. Jenuwein, T.; Laible, G.; Dorn, R.; Reuter, G. *Cell. Mol. Life Sci.* **1998**, *54*, 80.
3. Peters, A. H. F.; Kubicek, M. S.; Mechtler, K.; O'Sullivan, R. J.; Derijck, A. A. H. A.; Perez-Burgos, L.; Kohlmaier, A.; Opravil, S.; Tachibana, M.; Shinkai, Y.; Martens, J. H. A.; Jenuwein, T. *Mol. Cell* **2003**, *12*, 1577.
4. Rice, J. C.; Briggs, S. D.; Ueberheide, B.; Barber, C. M.; Shabanowitz, J.; Hunt, D. F.; Shinkai, Y.; Allis, C. D. *Mol. Cell* **2003**, *12*, 1591.
5. Tachibana, M.; Sugimoto, K.; Fukushima, T.; Shinkai, Y. *J. Biol. Chem.* **2001**, *276*, 25309.
6. Tachibana, M.; Sugimoto, K.; Nozaki, M.; Ueda, J.; Ohta, T.; Ohki, M.; Fukuda, M.; Takeda, N.; Niida, H.; Kato, H.; Shinkai, Y. *Genes Dev.* **2002**, *16*, 1779.
7. Tachibana, M.; Ueda, J.; Fukuda, M.; Takeda, N.; Ohta, T.; Iwanari, H.; Sakihama, T.; Kodama, T.; Hamakubo, T.; Shinkai, Y. *Genes Dev.* **2005**, *19*, 815.
8. Shankar, S. R.; Bahirvani, A. G.; Rao, V. K.; Bharathy, N.; Ow, J. R.; Taneja, R. *Epigenetics* **2013**, *8*, 16.
9. Fog, C. K.; Jensen, K. T.; Lund, A. H. *APMIS* **2007**, *115*, 1060.
10. Huang, J.; Dorsey, J.; Chuikov, S.; Zhang, X.; Jenuwein, T.; Reinberg, D.; Berger, S. L. *J. Biol. Chem.* **2010**, *285*, 9636.
11. Kondo, Y.; Shen, L. L.; Ahmed, S.; Boumber, Y.; Sekido, Y.; Haddad, B. R.; Issa, J. P. *PLoS One* **2008**, *3*, e2037.
12. Kondo, Y.; Shen, L. L.; Suzuki, S.; Kurokawa, T.; Masuko, K.; Tanaka, Y.; Kato, H.; Mizuno, Y.; Yokoe, M.; Sugauchi, F.; Hirashima, N.; Orito, E.; Osada, H.; Ueda, R.; Guo, Y.; Chen, X.; Issa, J. P.; Sekido, Y. *Hepatol. Res.* **2007**, *37*, 974.
13. Watanabe, H.; Soejima, K.; Yasuda, H.; Kawada, I.; Nakachi, I.; Yoda, S.; Naoki, K.; Ishizaka, A. *Cancer Cell Int.* **2008**, 8.
14. McGarvey, K. M.; Fahrner, J. A.; Greene, E.; Martens, J.; Jenuwein, T.; Baylin, S. B. *Cancer Res.* **2006**, *66*, 3541.
15. Trojer, P.; Zhang, J.; Yonezawa, M.; Schmidt, A.; Zheng, H.; Jenuwein, T.; Reinberg, D. *J. Biol. Chem.* **2008**, *284*, 8395.
16. Vedadi, M.; Barsyte-Lovejoy, D.; Liu, F.; Rival-Gervier, S.; Allali-Hassani, A.; Labrie, V.; Wigle, T. J.; Dimaggio, P. A.; Wasney, G. A.; Siarheyeva, A.; Dong, A.; Tempel, W.; Wang, S. C.; Chen, X.; Chau, I.; Mangano, T. J.; Huang, X. P.; Simpson, C. D.; Pattenden, S. G.; Norris, J. L.; Kireev, D. B.; Tripathy, A.; Edwards, A.; Roth, B. L.; Janzen, W. P.; Garcia, B. A.; Petronis, A.; Ellis, J.; Brown, P. J.; Frye, S. V.; Arrowsmith, C. H.; Jin, J. *Nat. Chem. Biol.* **2011**, *7*, 566.
17. Kubicek, S.; O'Sullivan, R. J.; August, E. M.; Hickey, E. R.; Zhang, Q.; Teodoro, M. L.; Rea, S.; Mechtler, K.; Kowalski, J. A.; Homon, C. A.; Kelly, T. A.; Jenuwein, T. *Mol. Cell* **2007**, *25*, 473.
18. Chang, Y.; Zhang, X.; Horton, J. R.; Upadhyay, A. K.; Spannhoff, A.; Liu, J.; Snyder, J. P.; Bedford, M. T.; Cheng, X. *Nat. Struct. Mol. Biol.* **2009**, *16*, 312.
19. Chiang, Y. K.; Kuo, C. C.; Wu, Y. S.; Chen, C. T.; Coumar, M. S.; Wu, J. S.; Hsieh, H. P.; Chang, C. Y.; Jseng, H. Y.; Wu, M. H.; Leou, J. S.; Song, J. S.; Chang, J. Y.; Lyu, P. C.; Chao, Y. S.; Wu, S. Y. *J. Med. Chem.* **2009**, *52*, 4221.
20. Sirci, F.; Goracci, L.; Rodriguez, D.; van Muijlwijk-Koezen, J.; Gutierrez-de-Teran, J.; Mannhold, R. *J. Comput. Aided Mol. Des.* **2012**, *26*, 1247.
21. Thangapandian, S.; John, S.; Sakkiah, S.; Lee, K. W. *Eur. J. Med. Chem.* **2010**, *45*, 4409.
22. *OMEGA, 2.4.6*; OpenEye Scientific Software: Santa Fe, NM, 2012.
23. *ROCS, 3.1.2*; OpenEye Scientific Software: Santa Fe, NM, 2012.
24. Feng, T. T.; Wang, H.; Zhang, X. J.; Sun, H. P.; You, Q. Y. *Med. Chem.* **2014**, *10*, 426.
25. Moffat, K.; Gillet, V. J.; Whittle, M.; Bravi, G.; Leach, A. R. *J. Chem. Inf. Model.* **2008**, *48*, 719.
26. Kirchmair, J.; Distinto, S.; Markt, P.; Schuster, D.; Spitzer, G. M.; Liedl, K. R.; Wolber, G. *J. Chem. Inf. Model.* **2009**, *49*, 678.
27. Tawa, G. J.; Baber, J. C.; Humblet, C. *J. Comput. Aided Mol. Des.* **2009**, *23*, 853.
28. Hawkins, P. C.; Skillman, A. G.; Warren, G. L.; Ellingson, B. A.; Stahl, M. T. *J. Chem. Inf. Model.* **2010**, *50*, 572.
29. Hawkins, P. C.; Nicholls, A. *J. Chem. Inf. Model.* **2012**, *52*, 2919.
30. Mani, T.; Wang, F.; Knabe, W. E.; Sinn, A. L.; Khanna, M.; Jo, I.; Sandusky, G. E.; Sledge, G. W., Jr.; Jones, D. R.; Khanna, R.; Pollok, K. E.; Meroueh, S. O. *Bioorg. Med. Chem.* **2013**, *21*, 2145.